Tubular Links for Eccentrically Braced Frames. II: Experimental Verification

Jeffrey W. Berman[1] and Michel Bruneau[2]

Abstract: This paper describes the results of an experimental study to verify proposed design requirements for eccentrically braced frame links with hollow rectangular (i.e., tubular) cross sections. Twelve primary link specimens and two supplementary links that have different end connections are tested. Three cross sections and four normalized link lengths are considered. Two of the cross sections have web and flange compactness ratios near the proposed limits while the third cross section has compactness ratios significantly less than the proposed limits. Shear, intermediate, and flexural, link lengths are tested, including some at the critical transition length from shear-to-intermediate link behavior. Results indicated that tubular links satisfying the proposed compactness and stiffener requirements can achieve the target plastic rotations for wide-flange links when subjected to the loading protocol specified in the 2005 AISC Seismic Provisions. The predominant failure mode is fracture of the link flange near the connection to the end plates used for testing. A method for calculating the ultimate link shear, proposed by others for wide-flange links, is also investigated and modified to agree with the results of the tubular link tests.

DOI: 10.1061/(ASCE)0733-9445(2008)134:5(702)

CE Database subject headings: Seismic design; Ductility; Steel structures; Experimentation; Steel frames; Bracing.

Introduction

Eccentrically braced frames (EBFs) with wide-flange (WF) links have been shown to have excellent seismic performance (Roeder and Popov 1978; Popov and Bertero 1980; Hjelmstad and Popov 1984; Malley and Popov 1984; Kasai and Popov 1986; Ricles and Popov 1989; Engelhardt and Popov 1992, among others). Recent research described in a companion paper (Berman and Bruneau 2008) and elsewhere (Berman and Bruneau 2005, 2006, 2007) has investigated the use of members with hollow rectangular (i.e., tubular) cross sections as links in EBFs, including a proof-of-concept experiment involving a full single-story EBF. As described in that research, tubular cross sections are not subject to lateral torsional buckling at typical EBF link lengths and, therefore, do not require lateral bracing. This makes tubular links desirable for applications such as bridge piers or elevator shafts, where lateral bracing of the link can be difficult to provide.

The companion paper described the development and results of a finite-element-element parametric study of links with tubular cross sections and various web and flange compactness ratios, link lengths, and stiffener conditions (a generic cross section with perimeter stiffeners is shown in Fig. 1). That study also investigated the use of hybrid cross sections, i.e., those with webs and flanges having different yield strengths. The results of that study were compactness and stiffener recommendations for links with tubular cross sections summarized in the conclusions of the companion paper.

Satisfying these compactness conditions resulted in link designs that were predicted (by nonlinear large displacement finite-element-element analysis) to be able to achieve the target plastic rotation capacities specified in the 2002 AISC Seismic Provisions (AISC 2002) prior to significant strength degradation from local buckling for web and flange yield strengths in the range of 250–450 MPa. Note that the same link behavior classification (i.e., shear, intermediate, and flexural) as used for WF shapes was found to be acceptable for tubular links. That classification is based on the normalized link length, ρ, defined as

$$\rho = \frac{e}{(M_p/V_p)} \tag{1}$$

where M_p and V_p=plastic moment and shear capacities of the cross section defined in Berman and Bruneau (2007) and e=link length. Shear links ($\rho \leq 1.6$) are dominated by shear yielding and the plastic rotation demand should be limited to 0.08 rad, flexural links ($\rho > 3.0$) are dominated by flexural yielding and should have plastic rotation demands limited to 0.02 rad, and intermediate links ($1.6 < \rho \leq 3.0$) have both significant shear and flexural yielding and plastic rotation demand should be limited to a value found via linear interpolation. The plastic rotation limits above are taken as the target plastic rotations for the links in this study.

This paper describes the experimental verification of the design recommendations for EBF links with tubular cross sections. First, the selection of three cross sections and four link lengths is discussed; this resulted in the consideration of 12 primary link specimen for testing. Two supplementary links having different

[1]Assistant Professor, Dept. of Civil and Environmental Engineering, More Hall 201-Box 352700, Univ. of Washington, Seattle, WA 98195-2700. E-mail: jwberman@u.washington.edu

[2]Director, Multidisciplinary Center for Earthquake Engineering Research, Professor, Dept. of Civil Structural and Environmental Engineering, Univ. at Buffalo, Amherst, NY 14260. E-mail: bruneau@mceermail.buffalo.edu

Note. Associate Editor: Benjamin W. Schafer. Discussion open until October 1, 2008. Separate discussions must be submitted for individual papers. To extend the closing date by one month, a written request must be filed with the ASCE Managing Editor. The manuscript for this paper was submitted for review and possible publication on June 15, 2006; approved on April 9, 2007. This paper is part of the ***Journal of Structural Engineering***, Vol. 134, No. 5, May 1, 2008. ©ASCE, ISSN 0733-9445/2008/5-702–712/$25.00.

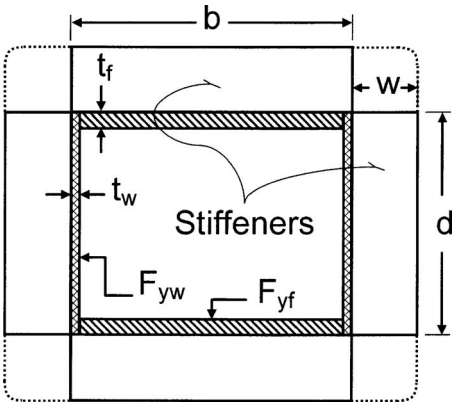

Fig. 1. Generic tubular cross section with perimeter stiffeners

end connections are also described. The experimental setup, instrumentation, and cyclic loading protocol are then presented. General experimental observations are provided, followed by a summary of the maximum plastic rotations achieved, and extrapolation of those results to the modified loading protocol in the 2005 AISC Seismic Provisions (AISC 2005). Next, the results for the supplementary links, one of which was tested under that new protocol, are described. Finally, observations regarding link overstrength and comparison with the overstrength formulation in Berman and Bruneau (2006) are provided. Note that this experimental investigation on links with tubular cross sections parallels an experimental investigation of WF links performed at the University of Texas at Austin (Okazaki et al. 2005) where similar conclusions regarding the effect of loading protocol on maximum plastic rotation capacity of links were drawn. Analytical extensions of that work were performed by Richards and Uang (2005).

Selection of Links

Primary Links

During the design procedure, A572 Grade 50 plate material with a nominal yield stress, F_y, of 345 MPa (50 ksi) and modulus of elasticity, E_s, of 2×10^5 MPa were assumed for both the webs and flanges of all three cross sections. Note that links with cross-section X2 had exterior stiffeners satisfying the requirements described in Berman and Bruneau (2006). The four normalized link lengths considered for each cross section were 1.2, 1.6, 2.1, and 3.0, which were also used in the finite-element-element parametric study.

Table 1. Properties of Link Test Specimens

	Cross section		
Quantity	X1	X2	X3
b (mm)	260.4	209.6	238.1
t_f (mm)	15.9	12.7	22.2
d (mm)	177.8	266.7	158.8
t_w (mm)	9.5	6.4	12.7
b'/t_f	15.2	15.5	9.6
b'/t_w	15.3	38	9
b/d	1.46	0.79	1.50
V_p (kN)	554	610	578
M_p (kN m)	265.7	296.7	277.7
F_{yw} (MPa)	480	475	430
F_{yf} (MPa)	371	430	365
F_{uw} (MPa)	516	496	501
F_{uf} (MPa)	489	501	490
V_{pa} (kN)	771	840	721
M_{pa} (kN m)	302.4	380.3	304.4

In addition to having cross sections and lengths meeting the above-presented descriptions, several practical issues associated with the test setup were also considered while selecting link specimen geometries. First, the capacity of the actuator and setup shown in Fig. 2 had to be sufficient to test the specimens to failure. Second, the cross sections were constrained to be similar in overall size so that, at most, two different connections to the setup were necessary. Finally, the number of setup configurations was limited to ensure that testing could be completed in a reasonable time period. Therefore, actual link lengths and expected maximum shear forces were selected to be as similar as possible for links having different cross sections and the same normalized link length.

Link specimens are denoted by cross-section number and normalized length, i.e., Specimen X1L1.2 has cross-section type 1 and a normalized length of 1.2. Table 1 gives cross-sectional properties for the links in this experimental study including compactness ratios, plastic shear forces, V_p, and plastic moments, M_p,

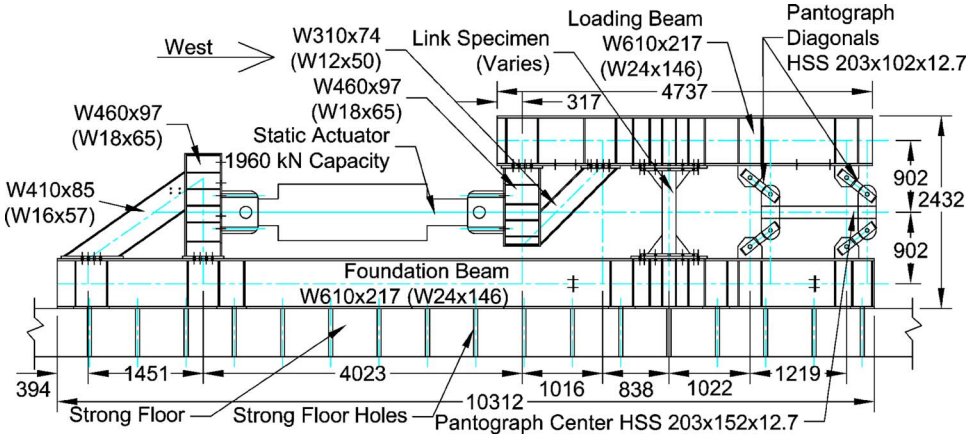

Fig. 2. Test setup for specimen with $\rho = 1.2$ and 1.6

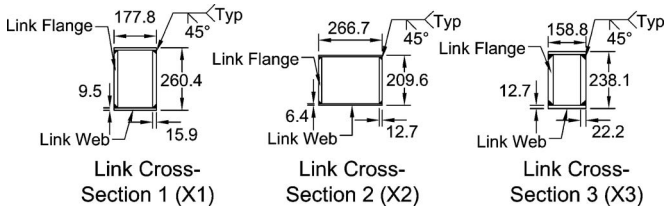

Fig. 3. Link cross sections

calculated using the nominal yield stress of 345 MPa. Fig. 3 shows the corresponding cross-section details. For all links, full penetration groove welds, similar to those used for the link in the proof-of-concept testing described in Berman and Bruneau (2007), were specified to assemble the hollow rectangular cross section. Note that the dimensions in Table 1 have been rounded to the nearest tenth of a millimeter (mm) and that U.S. customary units were used during the design process because of requirements from the fabricator. Further, note that the design link plastic shear forces in Table 1 are approximately three times that required for the two story pier in Pollino and Bruneau (2004) and approximately 1/4 and 2/5 of the design link shear forces for the links of the San Francisco-Oakland Bay Bridge piers and Richmond-San Rafael Bridge piers, respectively (Dusicka et al. 2002; Itani 1997).

As shown in the example elevation views of Specimens X1L1.2, X2L1.2, and X3L1.2, in Fig. 4, each link has a haunch at each end prior to the connection to an end plate. The primary reason for the haunch is to replicate the end condition of the link in the proof-of-concept testing described in Berman and Bruneau (2007), which was a full single-story EBF. There the link flanges were continuous through the end of the link and brace-to-link connection and terminate at the beam-to-column connections. That link had a gusset connection for each brace which was stiffened with a plate perpendicular to the link flange, referred to as the gusset stiffener, connected to the flange with a fillet weld. Fracture of the link flange occurred at the toe of this weld, in the heat affected zone (Berman and Bruneau 2007). The flange haunch, shown in cross sections at about midheight of the haunch in Fig. 5, also has a weld to the link flange that is perpendicular to the longitudinal axis of the link, although it is a significantly larger weld with larger heat input.

A secondary benefit of this haunch is to prevent fracture of the weld connecting the link to the end plate, which other researchers have reported in WF link testing. By increasing the depth and inertia of the cross section, the haunch reduces the stresses at the

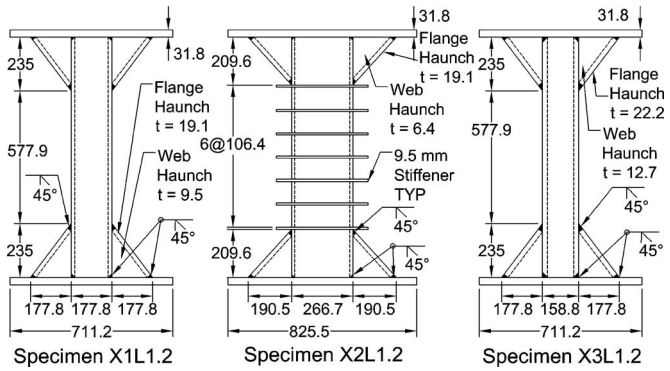

Fig. 4. Example specimen elevations

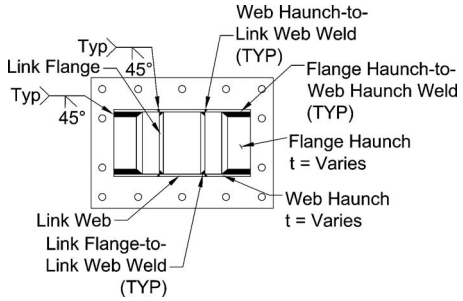

Fig. 5. Example cross section at haunch

end-plate connection. The flanges of the haunch for each cross section were designed such that the combined plastic moment capacity of the haunch and link flanges at the intersection with the end plate was at least twice the maximum anticipated end moment considering nominal yield stresses. The webs of the haunches were selected to be of the same thickness as the link webs for each cross section. As the link shear force is constant for the entire specimen length, including the haunches, the web haunches reduce the shear stress near the end plate. In all cases the active link length is taken to be the distance between the haunches.

Monotonic tension and cyclic tests were performed on coupons from the plate material used to fabricate the various link cross sections described earlier. The monotonic tension coupons conformed to ASTM A370. Results for web and flange yield and tensile strengths, F_{yw}, F_{yf}, F_{uw}, and F_{uf}, respectively, are given in Table 1. Note that the same plate material was used to fabricate the web of the X3 specimens and the flange of the X2 specimens. Table 1 also gives plastic shear, V_{pa}, and plastic moment, M_{pa}, values for each cross section calculated using the delivered material yield strengths and the equations presented in Berman and Bruneau (2007). The materials used for the webs of X1 and X2 specimens and for the flanges of the X2 specimens did not have a distinct yield plateau. Therefore, the 0.2% offset method was used to determine their yield stress. The thicker materials used for the flanges of the X1 and X3 specimens had a typical mild steel stress–strain curve with a yield plateau. Cyclic coupon test data for implementation in finite-element-element models of the links are given in Berman and Bruneau (2006).

Supplementary Links

The connection used for the preliminary links was judged to overly constrain plastic flow in the link flange at the intersection with the flange haunch plate and web haunch plate; thus, introducing high triaxial stresses in the web-to-flange welds of the links. This may have caused flange fracture to occur prior to some primary links achieving their target plastic rotation. Further, inspection of the fracture surfaces indicated that they likely initiated in the web-to-flange weld adjacent to the flange haunch and web haunch intersection. This observation contradicted the observation made regarding the flange fracture of the link in the proof-of-concept test in Berman and Bruneau (2007), where the fracture initiated in the flange itself, not in the web-to-flange weld.

Considering the issues regarding constraint of plastic flow in the flanges of the primary links, two supplementary link specimens were designed with an alternate connection to the end plates. These links used cross sections and link lengths identical to Specimens X1L1.6 and X2L1.6 with the alternate end-plate

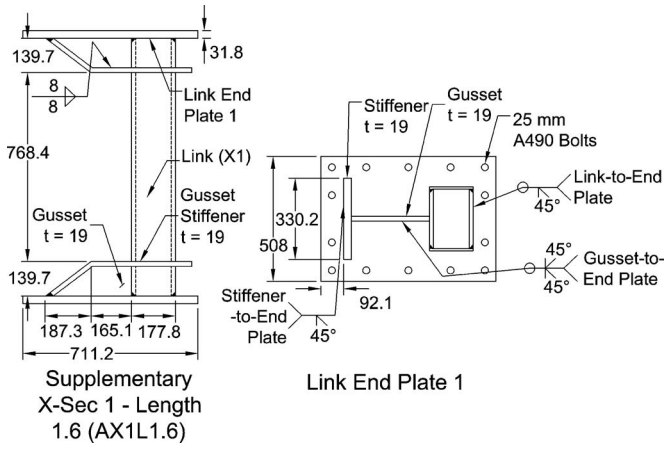

Fig. 6. Supplementary specimen and end plate

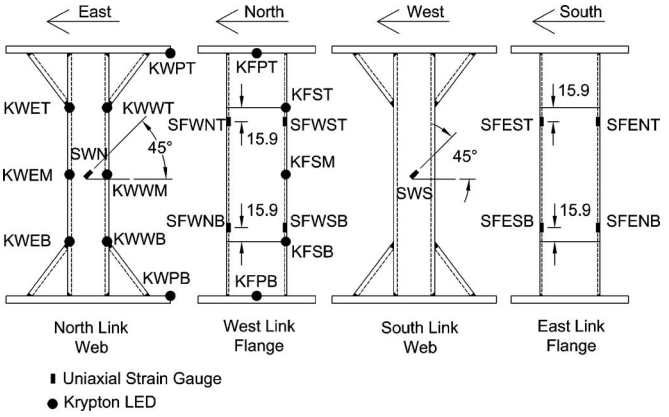

Fig. 7. Shear link instrumentation

connections shown in Fig. 6. The connections were designed to be similar to the link-to-brace connections used in the proof-of-concept test, i.e., with a single stiffened gusset at each link end that connects at midwidth of the flange, away from the web-to-flange welds. Further, the connection is not symmetric, in that the gusset is only located on one flange face, and the gusset stiffener is connected to the flange using fillet welds instead of full-penetration groove welds. Finally, the gusset stiffener is configured perpendicular to the longitudinal axis of the link, rather than at an inclined angle as was the case for the primary link specimens described in the previous section. Results for these supplementary links, denoted AX1L1.6 and AX2L1.6, will be reported with results for the primary links in the following sections.

Experimental Setup

The setup shown in Fig. 2 was designed to be reconfigurable to accommodate three different overall specimen lengths (including the link, haunches, and end plates). The shortest setup is shown in Fig. 2. All specimens with normalized link lengths of 1.2 and 1.6 had the same overall length of 1,111.3 mm, the specimens with normalized link lengths of 2.1 had overall lengths 1,435.1 mm, and the specimens with normalized link lengths of 3.0 had overall lengths of 1,949.5 mm. As the actuator extends or contracts, load is transferred on the west end of the actuator to the loading beam (LB) through the elbow connection. The result is uniform axial load and moment in the loading beam that is transferred as shear and end moment to the link and then to the foundation beam (FB) as axial load and moment. Note that the actuator force coincides with the link midpoint, resulting in equal and opposite link end moments and zero moment at the link midpoint, assuming rigid loading and foundation beams. At the east end of the actuator, the load is transferred to the FB through a similar elbow connection. The result is that the setup is a self-restrained reaction frame. Attachment to the strong floor was therefore designed only to resist uplift forces.

For all three setup configurations, the centerline of the actuator coincides with the link midpoint. Therefore, assuming rigid foundation and loading beams, the actuator load is equal to the link shear force and there is no load in the pantograph members (the pin-ended members at the west end of the test setup). The pantograph functions to prevent rotation of the loading beam while allowing the link to deform unrestrained in the axial and horizontal directions, preventing the introduction of axial load in the link when deformed in shear and flexure. Design loads for the pantograph members were calculated by considering a condition where the flanges at one end of the link fractured, resulting in zero moment capacity at that end and flexure in the loading beam which is resisted by the pantograph members. Additional details regarding the design of the test setup can be found in Berman and Bruneau (2006).

Instrumentation

Instrumentation for the link testing was designed such that key response parameters could be obtained from redundant data sources. For example, the link rotation could be calculated from both the Krypton Dynamic Measurement Machine (Metris 2005) and string displacement potentiometers. For brevity, only the strain gauge and krypton layouts are discussed here. Further information regarding the instrumentation can be found in Berman and Bruneau (2006).

Strain gauge layouts for the various links were designed to indicate the yielding sequence during testing and possibly provide useful information for future low cycle fatigue calculations. All gauges were high elongation EP-08-250-GB-120 gauges from Vishay Micro-Measurements, Inc. The layout for shear links is shown in Fig. 7 and involved gauges near the haunch end connections as well as at a 45° inclination angle on the webs at the link midpoint.

The Krypton Dynamic Measurement Machine is composed of three sensitive infrared cameras mounted on a moveable frame, numerous light-emitting diodes (LEDs), and an independent data acquisition system. LEDs are approximately 13 mm $(\frac{1}{2}$ in.) in diameter and can be attached to the specimen or test setup at any location visible to the cameras via hot glue, magnets, or other approaches. The three cameras then triangulate the location, velocity, and acceleration of the LEDs relative to a user defined coordinate system. Accuracy of the krypton is on the order of 0.1 mm and can be as high as 0.05 mm, depending on the distance from the camera to the LEDs. Placement of the LEDs is limited by the viewable window for the cameras, which increases as the distance between the LEDs and cameras increases.

LEDs were placed on all links as shown in Fig. 7. Numerous LEDs were placed on each specimen for redundancy, as attachment failure may occur under large strain conditions at the LED locations. Further, the LED layout on the specimens allows monitoring of possible twisting of the specimens during testing. Using

the LEDs at the top and bottom of the link, at two locations on the north web and one location on the west flange, the link rotation can be determined with triple redundancy from the krypton system and a fourth redundant measure from string pots (not shown).

Loading Protocol

The loading protocol used for testing 13 of the 14 hybrid rectangular link specimens is the one specified by the 2002 AISC Seismic Provisions (AISC 2002). It is the same protocol, based on total link rotation, that was used for the links in the finite-element-element parametric study described in Berman and Bruneau (2008). This loading protocol specifies three cycles at each of the total link rotation levels of 0.0025, 0.005, and 0.01 rad, followed by two cycles at each 0.01 rad increment, up to the maximum code specified rotation. However, for this testing program the loading was continued with two cycles at each 0.01 rad increment until failure. Displacement of the actuator was used as the control parameter during testing, which required that the specified rotation levels be converted into displacements using the link and setup geometries. For this purpose the haunch ends and setup were considered to be rigid and the actuator displacement was taken as the rotation times the link length. The flexibility of the setup caused the measured rotations to be somewhat less than the specified rotations in the protocol for all cases. Thus, the protocol was modified slightly during testing of some specimens to keep the measured rotations as near the desired rotations as practicable. Target plastic rotations are given in the seismic provisions based on link length. For links with a normalized length of 1.2 or 1.6, 2.1, and 3.0 the target is to achieve one complete cycle at 0.08, 0.08, 0.05, and 0.03 rad of total plastic rotation, respectively.

The supplementary link with cross-section 2, Specimen AX2L1.6, was tested using the loading protocol specified in the recent 2005 AISC Seismic Provisions (AISC 2005). This protocol was developed by Richards and Uang (2006) considering tabulated cumulative plastic rotation and cumulative energy dissipation demand from various eccentrically braced frames subjected to many ground motions. The protocol requires more cycles at lower rotation levels and fewer cycles at larger rotations relative to the protocol of the 2002 Seismic Provisions. Specifically it requires six cycles at 0.00375, 0.005, 0.0075, and 0.01 rad, four cycles at 0.015 and 0.02 rad, two cycles at 0.03 rad, one cycle at 0.04 and 0.05 rad, and then a single cycle at 0.02 rad increments from there. Similar assumptions to those described earlier were made for the calculation of actuator displacement for this protocol. The protocol was changed in light of the recent research (Richards and Uang 2006) and because the links at the transition length from shear to intermediate classification did not reach their target plastic rotation. Those links may have achieved their target plastic rotation had the 2005 AISC loading protocol been used as it requires fewer large rotation cycles. Further, experimental results in Okazaki et al. (2005) indicated that many WF links that failed to meet their target rotation under the 2002 loading protocol achieved significantly larger rotations under the revised loading protocol, achieving their target rotations.

Experimental Results

As discussed in the following, most of the primary links met their target plastic rotation with the exception of those links with $\rho = 1.6$ and one link with $\rho = 2.1$. Link shear force versus rotation

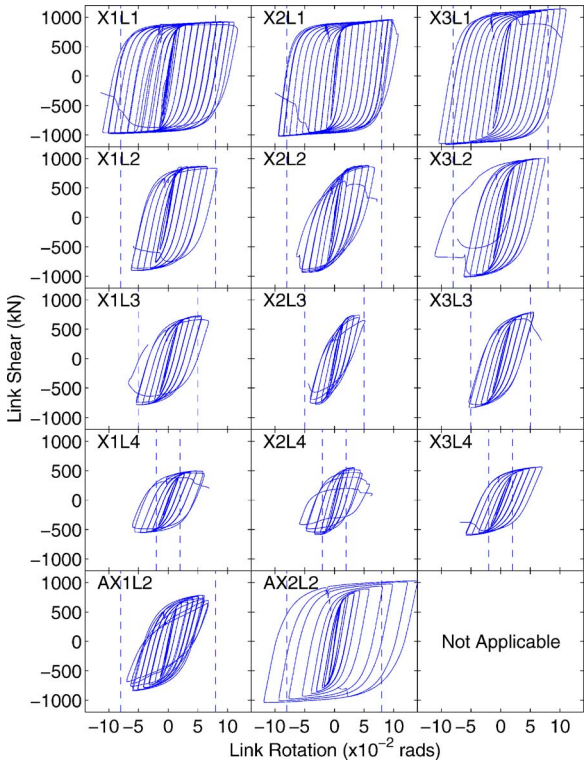

Fig. 8. Link shear force versus rotation hysteresis curves for all link specimens

hysteresis curves for all links, shown in Fig. 8, were generally symmetric, stable, and full prior to link fracture and an example of a deformed specimen is shown in Fig. 9 at 0.09 rad of total rotation. Note that in Fig. 8 the dashed lines indicate the target rotations for each link. All primary links had a failure mode of flange fracture near the flange haunch weld, which in all but two links occurred prior to 20% strength degradation from local buckling. A typical fracture is shown in Fig. 10(a) and the exposed surface is shown in Fig. 10(b). The fractures were found to originate, for the most part, in the web-to-flange weld adjacent to the web haunch. This is in contrast to the fracture of the flange in the proof-of-concept experiment, which was found to have originated in the flange itself. The difference is likely due to the web haunch plates located at the outer edges of the flange for the primary links, where the proof-of-concept test had a gusset at midwidth of the flange, away from the web-to-flange weld. Additionally, some specimens suffered local buckling prior fracture. Figs. 11(a and b) show local buckling of the web and flange of Specimen X2L3.0, respectively. Local buckling for that specimen did result in over 20% strength degradation prior to fracture. The results of a finite-element-element model of Specimen X2L3.0, developed in a similar manner to the models in the companion paper (Berman and Bruneau 2008), were in good agreement with the experimental results as shown in Fig. 12. Cumulative energy dissipation for the finite-element-element model of X2L3.0 over the life of the experimental specimen was within 16% of the experimental cumulative energy dissipation. In terms of limit plastic rotation the finite-element element model predicted degradation from local buckling somewhat earlier than observed in the experimental specimen; a limit plastic rotation of 0.025 rad was obtained from the finite-element element model whereas 0.035 rad was obtained experimentally. This comparison provides some confidence in the parametric study results regarding strength degradation from local

Fig. 9. Specimen X2L1.2 deformed at 0.09 rad

buckling. Similar agreement was observed for models of links that had local buckling degradation or no degradation prior to fracture. However, the analyses did not include fracture models, so degradation from fracture was not captured. For additional comparisons between finite-element element analyses and experimental, see Berman and Bruneau (2006).

Rotation Results

Table 2 contains the target plastic rotations, $\gamma_{p\text{targ}}$, and limit plastic rotations [i.e., the maximum rotation for which the links sustained full cycle of loading before 20% strength degradation occurred as described in Berman and Bruneau (2008)], γ_{plim}, and Fig. 13 shows the limit rotation for each link specimen versus normalized link length [including the supplementary links, AX1L1.6 and AX2L1.6, and the proof-of-concept link, the latter denoted POC1.3 which is described in Berman and Bruneau (2007)]. Note that plastic rotation is used here to be consistent with the maximum rotations allowed in the AISC seismic provisions which are specified in terms of plastic rotation. As shown, there are five links that did not achieve their target plastic rotation, namely, all three primary links with $\rho=1.6$, Specimen X2L2.1, and Specimen AX1L1.6. Recall that Specimen X2L2.1 did not satisfy the proposed design requirements because it had a web compactness ratio near $d'/t_w \leq 1.67\sqrt{E_s/F_{yw}}$, which exceeds the limit for intermediate links of $d'/t_w \leq 0.64\sqrt{E_s/F_{yw}}$ from Berman and Bruneau (2008). This leaves the three primary links with $\rho=1.6$ and the supplementary link, AX1L1.6, as the specimens that satisfied the proposed design requirements but did not achieve their target plastic rotation due to flange fracture.

It is interesting to note that the plastic rotation capacity of the links seems to increase with respect to normalized length when those lengths are above the transition point of intermediate to flexural behavior. This is logical considering that Richards (2004) postulated that the shear carried in a link's flange, which contributes to link overstrength, increases with decreasing link length. It follows that lower shear stresses are present in the flanges of flexural links, thereby reducing the triaxial stresses at the location of flange fracture, relative to the links with $\rho=2.1$ and 1.6. Further, the flexural links reached limit plastic rotations of more than twice the current plastic rotation limits. This is partly because the current limits for plastic rotation of flexural links were established from links where lateral torsional buckling was commonly the controlling failure mode. Here the links are self-stabilizing with respect to lateral torsional buckling, owing to their tubular cross section and, therefore, are able reach plastic rotations of more than twice the current 0.02 rad limit.

Links with $\rho=1.6$

As noted earlier, the primary links with $\rho=1.6$ satisfied the proposed design recommendations but did not achieve their target

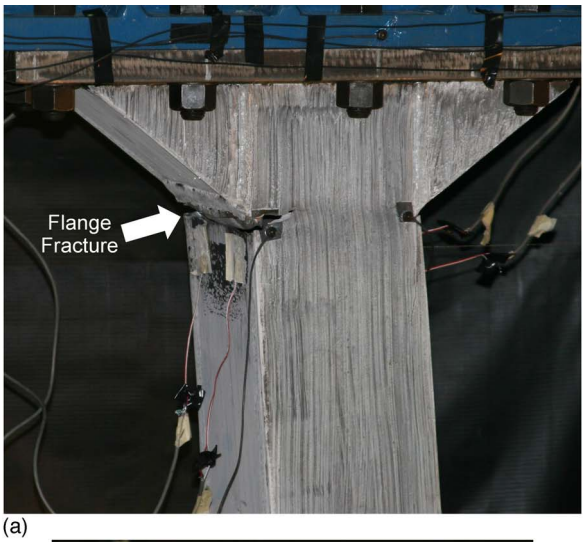

(a)

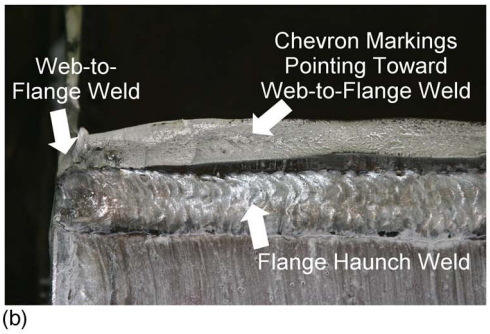

(b)

Fig. 10. (a) Example of flange fracture; (b) exposed fracture surface

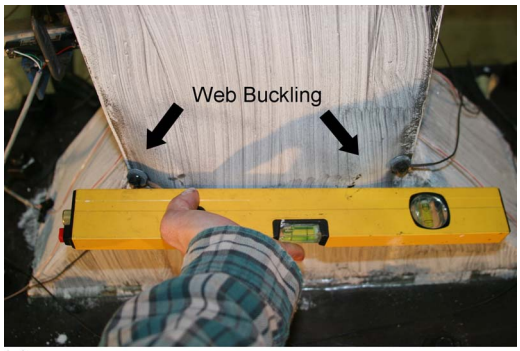

(a)

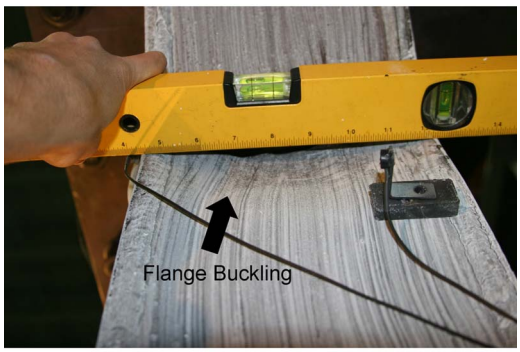

(b)

Fig. 11. Local buckling of Specimen X2L3.0; (a) web; (b) flange

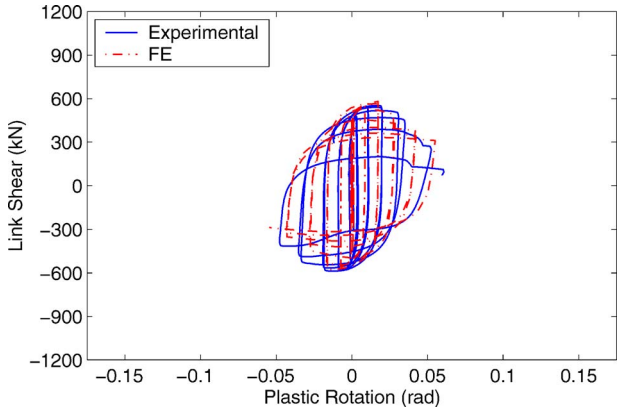

Fig. 12. Comparison of experimental and finite-element element hysteresis curves for Specimen X2L3.0

plastic rotation. Additionally, they were found to have considerably lower maximum plastic rotation and cumulative plastic rotation than links with $\rho=1.2$. There are two reasons for this that will be explored here and in later sections. The two aforementioned supplementary links were developed and tested to investigate these possible reasons for the links with $\rho=1.6$ suffering flange fracture prior to reaching their target plastic rotations.

The first reason considered here for primary links with $\rho=1.6$ not achieving their target plastic rotation is the combined effect of restraint of plastic flow in the flange caused by the rigid haunch end connection, and the large shear and flexural overstrength observed for links at this transition length. A second reason considered for the early fractures of the links with $\rho=1.6$ is that the loading protocol used for testing, from the 2002 AISC Seismic Provisions, is considerably more stringent than the new loading protocol specified in the 2005 AISC Seismic Provisions.

Considering the above-noted first reason, the flanges of the primary links tested here were subject to large triaxial stresses at the intersection with the haunch end connections, as the plastic flow in the flange was highly restrained at that location. However, the links with $\rho=1.6$ were also subjected to large shear forces, only slightly less than the similar links with $\rho=1.2$, and larger flexural demands associated with the longer link length, relative to the links with $\rho=1.2$. Therefore, it is conceivable that this combination of triaxial stresses and stresses from large strength demands could have caused flange fracture at lower plastic rotation levels relative to the links with $\rho=1.2$.

Extrapolation to New Loading Protocol

Research by Richards and Uang (2006) indicates that the loading protocol for EBF links in the 2002 AISC Seismic Provisions is overly demanding in terms of the number of high rotation cycles it requires. As such, they proposed a new loading protocol that has been adopted in the 2005 AISC Seismic Provisions that more realistically represents the maximum rotation demand EBF links must sustain. In light of this recent change, it is worthwhile to investigate what rotations might be achieved if the new loading protocol had been used for the testing of the hybrid rectangular links with haunch end connections. Further, as mentioned earlier, the difference in rotation demand for the loading protocols could provide insight into why the primary links with $\rho=1.6$ failed to reach their target plastic rotation. For reference, Fig. 14 shows the 2005 and 2002 loading protocols and the approximate yield rotation for all links of 0.01 rad. Note that a complete cycle without

Table 2. Experimental Results for All Link Specimens

Specimen	γ_{ptarg} (rad)	$\gamma_{p\ \mathrm{lim}}$ (rad)	$\gamma_{p\ \mathrm{lim}\ EH}$ (rad)	$\gamma_{p\ \mathrm{lim}\ RP}$ (rad)	$V_{\max}$ (kN)	$M_{\max}$ (kN m)
X1L1.2	0.08	0.090	0.182	0.182	981	283
X2L1.2	0.08	0.088	0.164	0.164	1,024	312
X3L1.2	0.08	0.087	0.163	0.163	1,164	336
X1L1.6	0.08	0.050	0.080	0.082	907	349
X2L1.6	0.08	0.040	0.060	0.079	936	360
X3L1.6	0.08	0.045	0.079	0.080	1,017	391
X1L2.1	0.05	0.038	0.058	0.076	781	394
X2L2.1	0.05	0.027	0.027	0.027	779	401
X3L2.1	0.05	0.037	0.056	0.056	831	419
X1L3.0	0.02	0.040	0.049	0.049	555	400
X2L3.0	0.02	0.035	0.035	0.054	587	429
X3L3.0	0.02	0.037	0.067	0.067	599	432
AX1L1.6	0.08	0.055	0.100	0.100	840	323
AX2L1.6[a]	0.08	0.115	0.115	0.115	1,041	410
POC1.3	0.08	0.105	0.137	0.137	750	172

[a]Specimen AX2L1.6 was tested under the 2005 loading protocol, therefore, the projected results for the 2005 loading protocol are the experimental results for that specimen.

significant strength degradation must be achieved at the target rotation for the link to be acceptable according to both provisions.

Using cumulative energy dissipation and/or cumulative plastic rotation, it is possible to estimate the plastic rotation that might have been achieved if the 2005 loading protocol had been used. These two parameters were chosen because they may be useful for fracture prediction using stress intensity factors or strain controlled low cycle fatigue, respectively. The procedure followed to achieve this prediction consists of the following steps:

1. Fit a cyclic numerical model, such as a bounding surface model, to the test results for each specimen. Fig. 15(a) shows a comparison of the experimental link shear force versus rotation hystereses for Specimen X1L1.6 with the one generated from application of a bounding surface model (Dafalias and Popov 1976).
2. For the rotations from the 2005 loading protocol, determine the corresponding link shear forces, using the cyclic model, to develop the approximate hysteresis that would be obtained for that protocol.
3. Find the cycle and corresponding rotation, using the 2005 loading protocol, for which the cumulative plastic rotation or cumulative energy dissipation equal the experimentally obtained maximum values. This is demonstrated using cumulative plastic rotation in Fig. 15(b) for Specimen X1L1.6.
4. Convert the corresponding maximum total rotation to plastic rotation by subtracting elastic component of rotation, which is the shear force divided by the initial stiffness.

Additional details on this procedure and the parameters used in the bounding surface model are given Berman and Bruneau (2006). This procedure is similar to one used in Richards and Uang (2003) for extrapolation of limit plastic rotations for WF links.

Table 2 gives the projected limit plastic rotations found using both cumulative energy dissipation, $\gamma_{p\mathrm{lim}EH}$, and cumulative plastic rotation, $\gamma_{p\mathrm{lim}RP}$, the limit plastic rotations from the experimental results, $\gamma_{p\mathrm{lim}}$, and the target plastic rotations, γ_{ptarg}. Figs. 16(a and b) show the projected plastic rotations versus the normalized link length considering cumulative energy dissipation and cumulative plastic rotation, respectively.

From Fig. 16(a) it is observed that all links are projected to reach their target plastic rotations under the 2005 loading protocol when cumulative energy dissipation is considered, except Specimens X2L1.6 and X2L2.1. As mentioned earlier, Specimen X2L2.1 does not satisfy the proposed design requirements, leaving X2L1.6 as the only specimen satisfying the proposed design

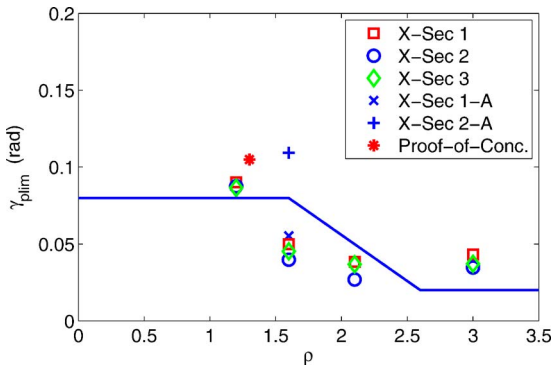

Fig. 13. Limit plastic rotation versus normalized length for all specimen tested (solid line=target rotation)

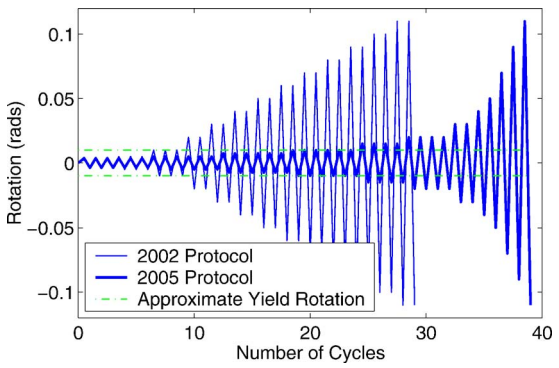

Fig. 14. Loading protocol comparison

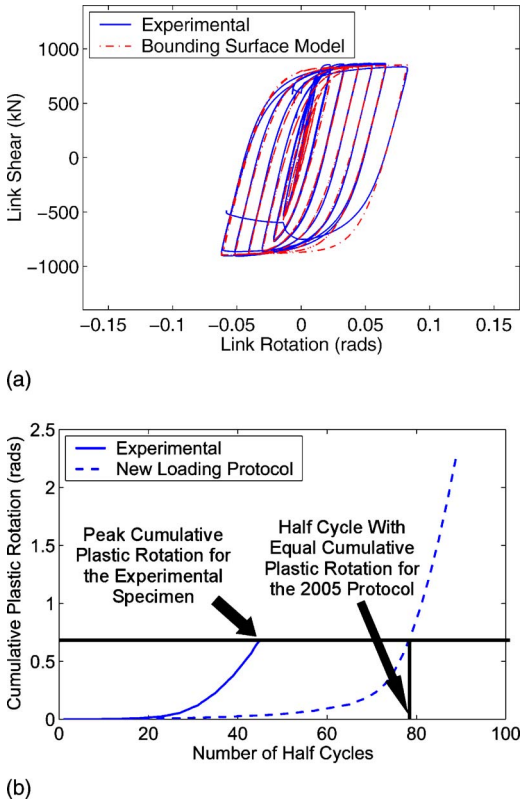

Fig. 15. Projection of results to 2005 loading protocol: (a) comparison of bounding surface model and experimental hysteresis curves; (b) determining half cycle where peak cumulative rotation is reached

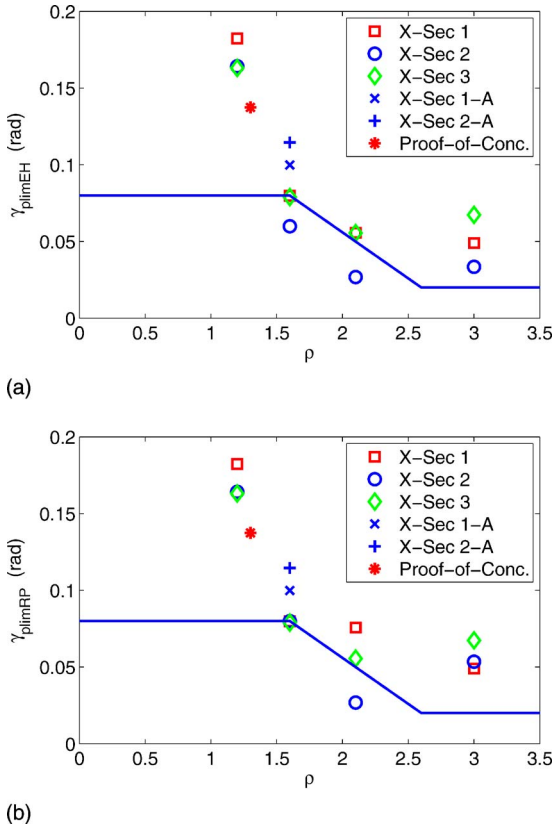

Fig. 16. Projected limit plastic rotation for 2005 loading protocol: (a) using cumulative energy dissipation; (b) using cumulative plastic rotation

requirements that is not projected to meet the target plastic rotation under the 2005 loading protocol considering cumulative energy dissipation. Additionally, Fig. 16(b) shows that the only link not projected to reach its target plastic rotation using cumulative plastic rotation is Specimen X2L2.1, which does not satisfy the proposed design requirements (Specimen X2L1.6 is projected to have a maximum plastic rotation of 0.079 rad, which for engineering purposes is approximately equal to the target 0.08 rad). Therefore, the proposed design requirements in Berman and Bruneau (2008) result in links that may achieve their target plastic rotation under the 2005 loading protocol. The supplementary link testing results presented in the following will provide more evidence for this conclusion considering cases where plastic flow at the flange ends is not as severely restrained. Further, these observations agree with those in Okazaki et al. (2005) where WF links were tested under both the 2002 and 2005 loading protocols and significantly larger maximum plastic rotations were achieved under the 2005 loading protocol.

Supplementary Links

Fig. 13 showed the experimental results for $\gamma_{p\text{lim}}$ versus ρ for all link specimens, including the supplementary specimens and proof-of-concept link (AX1L1.6, AX2L1.6, and POC1.3). From Fig. 13 and Table 2, it is observed that Specimen AX1L1.6 did not reach its target plastic rotation despite having an end connection that reduced the restraint against plastic flow at the flange ends. However, the failure mode for that specimen was not flange fracture but fracture of the gusset stiffener followed by failure of the welds connecting the link to end plate.

Fig. 13 and Table 2 also indicate that Specimens AX2L1.6 and POC1.3 reached limit plastic rotations of 0.115 and 0.105 rad, exceeding their target plastic rotation of 0.08 rad and the limit plastic rotation of Specimen X2L1.6. Recall that AX2L1.6 was tested using the 2005 loading protocol and had the same cross section as X2L1.6 but a different end connection. The plastic rotation projected for Specimen X2L1.6 with the 2005 loading protocol was 0.079 rad, whereas the maximum plastic rotation obtained for Specimen AX2L1.6 was 0.115 rad. Some of the difference between the projected results for Specimen X2L1.6 and the actual results for Specimen AX2L1.6 is likely due to the change in end connections. However, for this single data point, these results also indicate that the projection procedure is likely conservative, as it predicts a smaller maximum plastic rotation for Specimen X2L1.6 for the 2005 protocol than what was achieved with Specimen AX2L1.6.

Table 2 also gives the projected values of limit plastic rotation for the supplementary and proof-of-concept specimens considering both cumulative energy dissipation and cumulative plastic rotation. These values are also shown in Figs. 16(a and b) considering cumulative energy dissipation and cumulative plastic rotation, respectively. Note that the experimental data for Specimen AX2L1.6 are shown in Figs. 16(a and b) as it was tested using the 2005 loading protocol.

The change in end connection from Specimen X1L1.6 to Specimen AX1L1.6 resulted in only a slightly larger limit plastic rotation but considerably more cumulative plastic rotation. The change in loading protocol from the 2002 protocol for Specimen AX1L1.6 to the 2005 protocol for Specimen AX2L1.6 resulted in a significant increase in limit plastic rotation. These specimens

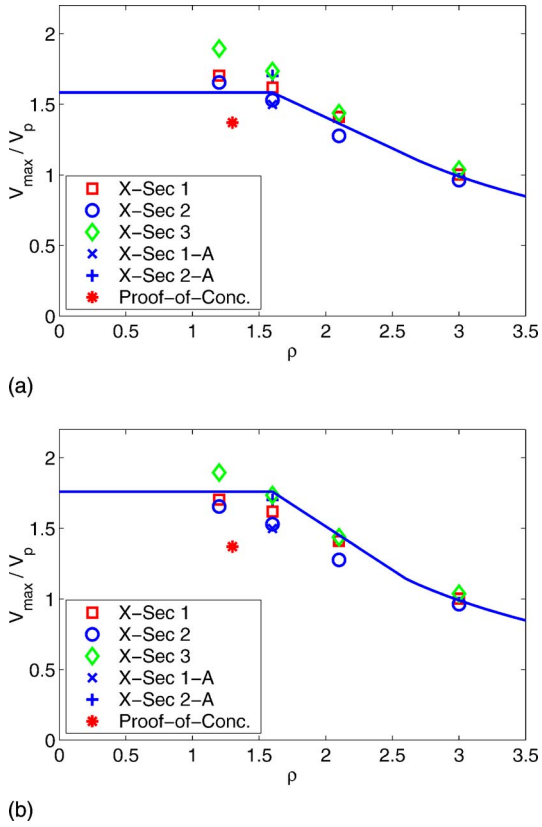

Fig. 17. Link overstrength (a) Ω as proposed by Richards and Uang (2002) for WF links; (b) Ω as modified here to match tubular link results

had the same cumulative plastic rotation and similar energy dissipation, yet Specimen AX2L1.6 reached a plastic rotation of 0.115 rad using the 2005 loading protocol whereas Specimen AX1L1.6 only reached 0.055 rad under the 2002 loading protocol. Additionally, the proof-of-concept link, which had a shorter normalized length than the supplementary specimens, achieved a plastic rotation of 0.105 rad using a loading protocol that is between the 2002 and 2005 loading protocols in terms of cumulative plastic rotation demand. Therefore, it seems that the difference in loading protocol intensity is largely responsible for the difference in obtained limit plastic rotations. This is similar to conclusions drawn by Okazaki et al. (2005) for WF links.

Considering the data presented, it appears that links satisfying the proposed design criteria will achieve their target plastic rotation if connections similar to the proof-of-concept test are used (i.e., connections that do not overly restrain the plastic flow in the link flanges), and if they are tested using the loading protocol from the 2005 AISC Seismic Provisions rather than the protocol from the 2002 provisions.

Overstrength Results

Table 2 has the maximum link shear forces, V_{max}, and maximum end moments, M_{max}, for all tested links. Table 1 gave design values for plastic shear, V_p, and plastic moment, M_p, calculated assuming 345 MPa (50 ksi) yield stresses. Fig. 17(a) shows the link overstrength values, where overstrength is defined as the maximum value from testing divided by the design value.

Richards (2004) developed a cyclic hardening factor that varies with the normalized link length and an equation for link plastic shear that accounts for the contribution of the flanges. This has been adapted to tubular links as shown in Berman and Bruneau (2006). Generally, the maximum link shear force expected to develop is

$$V_{ult} = \Omega R_y V_{pt} \tag{2}$$

where Ω=cyclic hardening factor and R_y=ratio of mean to nominal material yield stress (1.1 for A572 Grade 50 Steel). Note that the ratio of actual to nominal yield stresses for the webs of cross-sections X1, X2, and X3, were 1.39, 1.38, and 1.25, respectively, using the coupon test results reported earlier. Values above the code specified R_y value of 1.1 for A572 Grade 50 steel will be absorbed into the cyclic hardening factor, Ω. Applying the formulation of Richards results in the solid line in Fig. 17(a), where V_{pt} for links with $\rho \leq 1.6$ is now calculated by including the flange contribution, $2V_f$, in the plastic total shear as explained in Berman and Bruneau (2006). The figure shows that the Richards cyclic hardening factor, Ω, multiplied by R_y, and indicated by the solid line, reasonably predicts link overstrength for longer links but underestimates overstrength for short links, particularly when $\rho = 1.2$.

A more conservative formulation of the cyclic hardening factor can be achieved by changing the definition of the cyclic hardening factor from that of Richards (2004), which was proposed for WF links, to

$$\Omega = 1.6, \quad \rho \leq 1.6$$

$$\Omega = 1.6 - 0.56(\rho - 1.6), \quad 1.6 < \rho \leq 2.6$$

$$\Omega = 2.7/\rho, \quad \rho \geq 2.6 \tag{3}$$

This slightly modified version of the cyclic hardening factor results in a more conservative approximation of the overstrength observed for the tubular links tested here, as shown in Fig. 17(b).

Conclusions

A self-stabilizing link for eccentrically braced frames utilizing a tubular cross section has been developed. Here, experimental results for 14 tubular link specimens tested under cyclic quasistatic loading are presented, and performance is assessed. The tubular link cross sections were designed to examine proposed design requirements developed from a finite-element element parametric study. For webs of tubular sections used as shear links, a considerably larger web compactness ratio limit is proposed relative to that currently allowed by AISC, as long as stiffeners are present. Proposed stiffener spacing for tubular links is also different from the current requirements for links utilizing wide-flange shapes in that they are only required for shear links, not intermediate and flexural links. Links meeting the proposed web and flange compactness criteria were shown to have the ductility necessary to achieve their target plastic rotations under the loading specified by the 2005 AISC Seismic Provisions. The experimental results also allowed the overstrength of the tubular links to be quantified as a function of their normalized link length.

Most link specimens investigated suffered flange fracture at large rotations. This failure mode was largely attributed to significant restraint against plastic flow in the flange at the intersection with the link end connection. Therefore, link end connections that minimize this restraint, such as the type used in the supplementary links reported here, are recommended.

Acknowledgments

This research was conducted by the State University of New York at Buffalo and was supported by the Federal Highway Administration under Contract No. DTFH61-98-C-00094 and the Multidisciplinary Center for Earthquake Engineering Research. However, any opinions, findings, conclusions, and recommendations presented in this paper are those of the writers and do not necessarily reflect the views of the sponsors.

References

AISC. (2002). *Seismic provisions for structural steel buildings*, Chicago.

AISC. (2005). *Seismic provisions for structural steel buildings*, Chicago.

Berman, J. W., and Bruneau, M. (2005). "Approaches for the seismic retrofit of braced steel bridge piers and proof-of-concept testing of a laterally stable eccentrically braced frame." *Technical Rep. No. MCEER-05-0004*, Multidisciplinary Center for Earthquake Engineering Research, Buffalo, N.Y.

Berman, J. W., and Bruneau, M. (2006). "Further development of tubular eccentrically braced frame links for the seismic retrofit of braced steel truss bridge piers." *Technical Rep. No. MCEER-06-0006*, Multidisciplinary Center for Earthquake Engineering Research, Buffalo, N.Y.

Berman, J. W., and Bruneau, M. (2007). "Experimental and analytical investigation of tubular links for eccentrically braced frames." *Eng. Struct.*, 29(8), 1929–1938.

Berman, J. W., and Bruneau, M. (2008). "Tubular links for eccentrically braced frames. I: Finite element parametric study." *J. Struct. Eng.*, 134(5), 692–701.

Dafalias, Y. F., and Popov, E. P. (1976). "Plastic internal variables formalism of cyclic plasticity." *J. Appl. Mech.*, 43(4), 645–651.

Dusicka, P., Itani, A. M., and Buckle, I. G. (2002). "Cyclic behavior of shear links and tower shaft assembly of San Francisco-Oakland Bay Bridge Tower." *Technical Rep. No. CCEER 02-06*, Center for Civil Engineering Earthquake Research, Univ. of Nevada, Reno, Reno, Nev.

Engelhardt, M. D., and Popov, E. P. (1992). "Experimental performance of long links in eccentrically braced frames." *J. Struct. Eng.*, 118(11), 3067–3088.

Hjelmstad, K. D., and Popov, E. P. (1984). "Characteristics of eccentrically braced frames." *J. Struct. Eng.*, 110(2), 340–353.

Itani, A. M. (1997). "Cyclic behavior of Richmond-San Rafael Tower Links." *Technical Rep.* No. *CCEER 97-4*, Center for Civil Engineering Earthquake Research, Univ. of Nevada, Reno, Reno, Nev.

Kasai, K., and Popov, E. P. (1986). "General behavior of WF steel shear link beams." *J. Struct. Eng.*, 112(2), 362–382.

Malley, J. O., and Popov, E. P. (1984). "Shear links in eccentrically braced frames." *J. Struct. Eng.*, 110(9), 2275–2295.

Metris, Inc. (2005). K-Series cameras by Metris, Inc., ⟨www.metris.com⟩.

Okazaki, T., Arce, G., Ryu, H. C., and Engelhardt, M. D. (2005). "Experimental study of local buckling, overstrength, and fracture of links in eccentrically braced frames." *J. Struct. Eng.*, 131(10), 1526–1535.

Pollino, M., and Bruneau, M. (2004). "Seismic retrofit of bridge steel truss piers using a controlled rocking approach." *Technical Rep. No. MCEER-04-0011*, Multidisciplinary Center for Earthquake Engineering Research, State Univ. of New York at Buffalo, Buffalo, N.Y.

Popov, E. P., and Bertero, V. V. (1980). "Seismic analysis of some steel building frames." *J. Engrg. Mech. Div.*, 106(1), 75–92.

Richards, P. (2004). "Cyclic stability and capacity design of steel eccentrically braced frames." Ph.D. dissertation, Univ. of California, San Diego.

Richards, P., and Uang, C. M. (2003). "Development of testing protocol for short links in eccentrically braced frames." *Rep. No. SSRP-2003/08*, Structural Systems Research Project, Dept. of Structural Engineering, Univ. of Californi, San Diego, La Jolla, Calif.

Richards, P., and Uang, C. M. (2005). "Effect of flange width-thickness ratio on eccentrically braced frames link cyclic rotation capacity." *J. Struct. Eng.*, 131(10), 1546–1552.

Richards, P., and Uang, C. M. (2006). "Testing protocol for short links in eccentrically braced frames." *J. Struct. Eng.*, 132(8), 1183–1191.

Ricles, J. M., and Popov, E. P. (1989). "Composite action in eccentrically braced frames." *J. Struct. Eng.*, 115(8), 2046–2066.

Roeder, C. W., and Popov, E. P. (1978). "Eccentrically braced steel frames for earthquakes." *J. Struct. Div.*, 104(3), 391–412.